

Conductance Fluctuations in Disordered 2D Topological Insulator Wires: From Quantum Spin-Hall to Ordinary Phases

Hsiu-Chuan Hsu¹, Ioannis Kleftogiannis¹, Guang-Yu Guo^{1,2}, Víctor A. Gopar³

¹*Department of Physics, National Taiwan University, Taipei 10617, Taiwan*

²*Physics Division, National Center for Theoretical Sciences, Hsinchu 30013, Taiwan*

³*Departamento de Física Teórica and BIFI, Universidad de Zaragoza, Pedro Cerbuna 12, E-50009, Zaragoza, Spain*

Impurities and defects are ubiquitous in topological insulators (TIs) and thus understanding the effects of disorder on electronic transport is important. We calculate the distribution of the random conductance fluctuations $P(G)$ of disordered 2D TI wires modeled by the Bernevig-Hughes-Zhang (BHZ) Hamiltonian with realistic parameters. As we show, the disorder drives the TIs into different regimes: metal (M), quantum spin-Hall insulator (QSHI), and ordinary insulator (OI). By varying the disorder strength and Fermi energy, we calculate analytically and numerically $P(G)$ across the entire phase diagram. The conductance fluctuations follow the statistics of the unitary universality class $\beta = 2$. At strong disorder and high energy, however, the size of the fluctuations δG reaches the universal value of the orthogonal symmetry class ($\beta = 1$). At the QSHI-M and QSHI-OI crossovers, the interplay between edge and bulk states plays a key role in the statistical properties of the conductance.

1. Introduction

Topological insulators (TIs) are currently at the forefront of fundamental research in condensed matter physics and their singular electronic properties, such as the existence of dissipationless helical edge states, make them potential candidates for practical uses in low power consumption and spin-based electronic devices.¹⁾ Thus, an extensive literature covering fundamental and practical aspects of TIs already exists.²⁻⁵⁾ Most of the studies have been concentrated on pristine TIs, although the presence of disorder, such as impurities or lattice imperfections, is unavoidable in real devices.

The helical edge states of TIs are insensitive to weak disorder due to time-reversal (TR) symmetry, but strong disorder can still affect the electronic transport properties of TIs, as was recently demonstrated.⁶⁻⁹⁾ For instance, the stability of the edge states in the presence of

disorder has been studied in two-dimensional (2D) TIs and an unexpected quantum phase, the topological Anderson insulator, was discovered.^{6,7)} Effects of disorder in three-dimensional TIs have been also investigated within the Aharonov-Bohm oscillations phenomenon.¹⁰⁻¹³⁾

Disorder effects in low dimensional electronic devices have been a fundamental issue since early studies in the field of mesoscopic physics, particularly concerning the problem of quantum transport.^{14,15)} It is known that multiple coherent scattering of electrons through disordered quantum wires can give a universal character to the transport in the sense that the statistical properties of the conductance fluctuations depend on few and general physical parameters of the system, such as TR and spin-rotation symmetries, whereas microscopic details are irrelevant. One known result on this respect is the constant value of the standard deviation of the conductance fluctuations in the diffusive regime, the so-called universal conductance fluctuations (UCF),¹⁶⁾ depending only on the presence of TR and spin-rotation symmetries: the UCF takes the value $\sqrt{8/15\beta}$, for $\beta = 1, 2,$ and 4 . The symmetry class $\beta = 1$ corresponds to systems that preserve both TR and spin-rotation symmetries, while $\beta = 2$ designates the cases with broken TR symmetry. If TR symmetry is preserved, but spin-rotation symmetry is broken, we have the symmetry class $\beta = 4$.¹⁵⁾ Therefore, a statistical study of the conductance fluctuations is naturally linked to the presence of disorder and symmetries play a fundamental role in the analysis.

Moments of the conductance random fluctuations such as the average and variance have been recently experimentally and theoretically investigated in TIs.^{7,17-22)} Although these two conductance moments provide important statistical information, they might not be sufficient for a full statistical description, especially when large conductance fluctuations are present, as frequently happens in experiments. A complete statistical description of the conductance fluctuations is provided by the full distribution of the conductance. To the best of our knowledge, few works have been devoted to the study of the distribution of the conductance fluctuations in TIs.^{23,24)} In Ref. 23, the conductance fluctuations in a quantum network model are analyzed via the distribution of transmission eigenvalues, while in Ref. 24 the Bernevig-Hughes-Zhang (BHZ) tight-binding model has been considered to study numerically the conductance distribution in topological Anderson insulators. Thus, a thorough theoretical analysis of the conductance fluctuation in 2D TI is needed.

In this work, we first calculate the conductance distributions of disordered 2D TI wires modeled by the BHZ Hamiltonian describing an inverted InAs/GaSb quantum-well known for its practical advantages over other 2D TI materials, including the well-developed material control for fabrication and the tunable band structure by electric fields.^{25,26)} We obtain the

phase diagrams of the mean and standard deviation of the conductance, which reveal three different quantum phases or regimes: the metallic (M), the ordinary insulating (OI), and the quantum spin-Hall insulating (QSHI) phase. Secondly, to get a full understanding of the statistical properties in each regime and at the crossovers, we perform a theoretical analysis based on random matrix theory (RMT).^{27,28)} We find that the conductance fluctuations for 2D TI wires follow the $\beta = 2$ symmetry class in all the phases and crossovers except in the strongly disordered metallic region, where the UCF approach the value of the symmetry class $\beta = 1$.

At the M-QSHI crossover regime, we need to take into account the different extents of localization of the conducting channels to describe the asymmetric distribution centered around the average conductance $\langle G \rangle = 2$. For simplicity, the unit of the conductance of e^2/h is omitted throughout this paper. Similarly, as the system is driven from the QSHI to the OI regime, the conductance deviates significantly from $G = 2$, although its fluctuations can be described as in the OI phase. Our analysis reveals that the edge states play an important role at the crossover regimes that involve the QSHI phase and the symmetry of the Hamiltonian alone is not enough to obtain a full understanding of the statistical properties of the conductance.

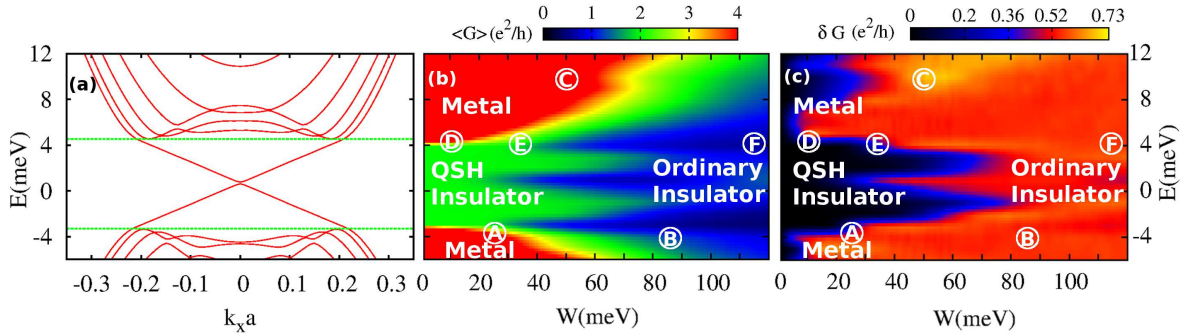


Fig. 1. (Color online) (a) The band structure of an InAs/GaSb nanowire with $N = 60$. The green dashed lines indicate the energy range where helical edge states occur. The phase diagrams of (b) the mean conductance $\langle G \rangle$ and (c) the standard deviation δG in the $E - W$ plane using 5000 disorder configurations. Circled letters denote the points where conductance distributions are calculated, as shown in Figs. 2, 4, and 5.

2. Hamiltonian Model

We adopt the BHZ model in the tight-binding representation to describe the electronic properties of the clean InAs/GaSb TI wires.^{6,26,29)} The Hamiltonian H consists of two terms: $H = H_c + H_d$, where H_c corresponds to a clean (disorder free) TI wire, and H_d contains a

source of disorder. The H_c term can be written in a block diagonal form as

$$H_c = \sum_{ip} V c_{ip}^\dagger c_{ip} + t_{xp} c_{ip}^\dagger c_{i+\delta x,p} + t_y c_{ip}^\dagger c_{i+\delta y,p} + h.c. \quad (1)$$

$$V = \begin{pmatrix} -4D + M - 4B & 0 \\ 0 & -4D - M + 4B \end{pmatrix} \quad (2)$$

$$t_{xp} = \begin{pmatrix} D + B & -iAp/2 \\ -iAp/2 & D - B \end{pmatrix} \quad (3)$$

$$t_y = \begin{pmatrix} D + B & A/2 \\ -A/2 & D - B \end{pmatrix}, \quad (4)$$

where $p = \pm$ denotes the pseudo spin, $i = (x, y)$ is the site index and $\delta x(y)$ is the vector to the nearest neighbor along the $x(y)$ -direction. The matrices V, t_{xp}, t_y are in the basis of electron and hole states. The parameters A, B, D, M are material-dependent. We use the values for those parameters of a InAs/GaSb quantum well derived from $k \cdot p$ method:^{26,29)} $A = 18.5$ meV, $B = -165$ meV, $D = -14.5$ meV, $M = -7.8$ meV with the lattice constant $a = 2$ nm. The Hamiltonian preserves time-reversal symmetry that prevents backscattering of the edge states³⁰⁾ as well as the structural and bulk inversion symmetries. Since we focus on the quantum spin-Hall edge transport, which is protected by the energy gap, the inversion asymmetries are neglected for simplicity.^{26,29)}

A source of disorder is introduced in the Hamiltonian model in a standard way by considering a random on-site energy:

$$H_d = \sum_{ip} \epsilon_i c_{ip}^\dagger I c_{ip} \quad (5)$$

where ϵ_i is a random number uniformly distributed in the range $[-W/2, W/2]$ and I is the 2×2 identity matrix. Although we have neglected other sources of disorder that affect the scattering processes such as electron-electron interactions or random fluctuations in the spin-orbit interaction,³¹⁾ we expect that this short-range disorder within a single-electron picture captures fundamental physical information of realistic systems. See for instance Ref. 13.

The above BHZ tight-binding Hamiltonian model is solved numerically and the conductance G is calculated by attaching a perfect lead to each side of the InAs/GaSb wire. Within the Landauer-Büttiker formalism³²⁾ the conductance is given by $G = \frac{2e^2}{h} \sum_i^n \tau_i$, where τ_i are the transmission eigenvalues of tt^\dagger , t being the $n \times n$ transmission matrix calculated by the recursive Green's function method^{32,33)} with $n = 2N$, where N is the width of the wire in units of the lattice constant.

3. Results and Discussion

3.1 Phase Diagrams

First we show the band structure of a pristine InAs/GaSb wire in Fig. 1(a). Unless stated otherwise, we set the number of sites along the y - and x -direction to $N = 60$ and $L = 300$, respectively, and assume the transport to be along the x -direction. The edge states occur in the energy window $[-3.36, 4.55]$ meV. The presence of disorder, however, changes the quantum phase of TIs and some signatures of these phases can be seen in the phase diagram of the ensemble average conductance $\langle G \rangle$ in the energy-disorder strength ($E - W$) plane [see Fig. 1 (b)]. From this phase diagram, we can identify the QSHI phase characterized by the average value $\langle G \rangle = 2$, in the energy range of $[-3.36, 4.55]$ meV (green area) and up to a disorder strength $W = 40$ meV, approximately. If the energy is increased, within the same range of disorder strength, the TI wire changes to the metallic regime, whereas if the strength of disorder is increased within the energy window $[-3.36, 4.55]$ meV, the TI wire becomes an ordinary insulator ($\langle G \rangle < 1$).

Further useful information can be obtained by plotting the standard deviation of the conductance $\delta G = \sqrt{\langle (G - \langle G \rangle)^2 \rangle}$ in the $E-W$ plane. From the δG phase diagram shown in Fig. 1 (c), we observe that for energies in $[-3.36, 4.55]$ meV and until disorder strength $W = 40$ meV (black region) the conductance fluctuations are negligible, revealing the robustness of the edge states against disorder in the QSHI regime. For higher energies, however, the standard deviation takes the UCF value $\delta G = \sqrt{4/15} \approx 0.52$, which is the representative value of the metallic phase for $\beta = 2$. We notice, however, that at strong disorder strength and high energy, δG reaches the value 0.73 (yellow region in Fig. 1 (c)), which corresponds to the UCF for the symmetry class $\beta = 1$.

Once we have identified the strength of disorder and energy intervals where the different phases of the TI lie, we proceed to perform a statistical analysis of the conductance fluctuations in each regime.

3.2 Metal - Ordinary Insulator Crossover

We first study the evolution of the conductance distribution from the M to the OI regimes as the strength of disorder increases. In Fig. 2 (a), we show $P(G)$ for three different values of the W at fixed energy $E = -4$ meV. The histograms are obtained by numerical calculation using 10000 disorder realizations. In the M regime, at disorder $W = 24$ meV, the conductance distribution follows the expected Gaussian distribution (solid line). The variance of the

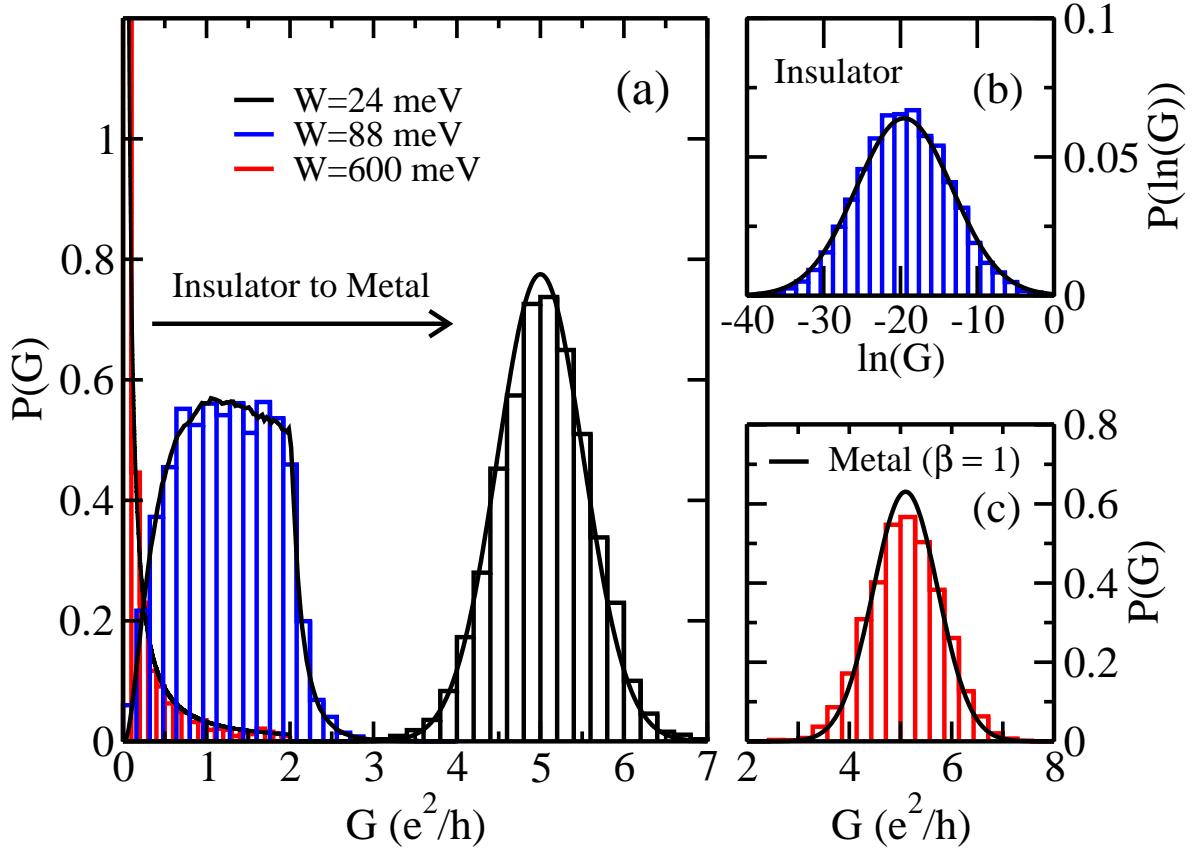


Fig. 2. (Color online) (a) Conductance distributions at $E = -4$ meV for different disorder strengths W showing the crossover from M to OI phase. $W = 24/88$ meV corresponds to the point (A)/(B) in the phase diagrams in Fig. 1. The mean conductance $\langle G \rangle = 5, 1.2, 0.07$ for $W = 24, 88$ and 600 meV, respectively. (b) The log-normal distribution for the OI phase at $E = -4, W = 1000$ meV ($\langle G \rangle = 5 \times 10^{-4}, \langle \ln(G) \rangle = -19.5$). (c) Conductance distribution of the point (C) in the phase diagrams in Fig. 1. The solid line corresponds to a Gaussian distribution with variance $8/15$ (as in the $\beta = 1$ symmetry class) and average conductance 5.1 .

Gaussian distribution is given by the UCF: $\sqrt{4/15}$, i.e., $P(G)$ is given by:

$$P(G) = \sqrt{\frac{15}{8\pi}} e^{-\frac{15}{8}(G-\langle G \rangle)^2} \quad (6)$$

with $\langle G \rangle = 5$ for the case shown in Fig. 2 (a).

We note that the value of the UCF ($\sqrt{4/15}$) corresponds to the physical systems with broken TR symmetry, i.e., $\beta = 2$ universality class. Indeed, each block in the Hamiltonian breaks TR symmetry and it thus belongs to the $\beta = 2$ symmetry, i.e., the conductance G is given by the identical contribution of the two Hamiltonian blocks with $\beta = 2$ symmetry class. Moreover, the block diagonal form of the Hamiltonian is a consequence of the inversion symmetry present in our model.^{5,34)}

As the strength of disorder is increased, the Gaussian distribution becomes wider and the

Gaussian landscape is lost. As an example, in Fig. 2 (a) we show the distribution $P(G)$ in this crossover between the M and OI regime (blue histogram), at disorder strength $W = 88$ meV . In this case, the conductance fluctuations are large; in particular, for the case shown in Fig. 2 (a), the relative fluctuations $\delta G/\langle G \rangle$ are five times larger than in the previous metallic phase (black histogram). The theoretical curve (solid line) that describes the numerical simulations (blue histogram) has been obtained from the joint distribution $P_s(\{\tau_i\})$ ($i = 1, 2, \dots, n$) of the different transmission eigenvalues τ_i together with the Landauer-Büttiker expression for the conductance, as follows. Within the Dorokhov-Mello-Pereyra-Kumar approach,²⁷⁾ the joint distribution for disordered wires supporting n transmission channels, $P(\{\tau_i\})$ where τ_i are the eigenvalues of the transmission matrix, follows a diffusion equation which describes the evolution of $P(\{\tau_i\})$ with the system length. For the unitary symmetry class $\beta = 2$, $P(\{\tau_i\})$ is conveniently written in terms of the variables $x_i = \text{acosh}[1/\sqrt{\tau_i}]$ as,³⁵⁾

$$p(\{x_i\}) = \frac{1}{Z} \exp[-H(\{x_i\})], \quad (7)$$

where $Z = \int \prod_i dx_i \exp[-H(\{x_i\})]$ and $H(x_i) = \sum_{i < j} u(x_i, x_j) + \sum_i V(x_i)$.

In both the metallic and ordinary insulating regimes, the functions $u(x_i, x_j)$ and $V(x_i)$ can be written as:^{35,36)}

$$\begin{aligned} u(x_i, x_j) &= \ln |\sinh^2 x_i - \sinh^2 x_j| + \ln |x_i^2 - x_j^2|, \\ V(x_i) &= ns^{-1}x_i^2 - \frac{1}{2} \ln |x_i \sinh 2x_i|, \end{aligned} \quad (8)$$

where $s = L/nl$, l being the mean free path and n the number of conducting channels. We point out that the ratio s is the only microscopic information that plays a role in the above model and can be determined by the mean conductance $\langle G \rangle$. For instance, in the metallic limit, $\langle G \rangle = \xi/L$, where ξ is the localization length equaling to nl , while in the ordinary insulating limit, $\langle G \rangle = e^{-\xi/L}$. In our analysis, s is set to a value that reproduce $\langle G \rangle$, obtained from the numerical simulations.

Using the joint distribution $P(\{\tau_i\})$ (or equivalently $p(\{x_i\})$) we calculate the conductance distribution which is given by

$$P(G) = \langle \delta(G - 2 \sum_i^n \tau_i) \rangle, \quad (9)$$

where the brackets represent the average performed with the probability density function $p(\{x_i\})$, Eq. (7). Thus, $P(G)$ in Eq. (9) can be calculated by numerical integration.

For the crossover regime shown in Fig. 2 (a), the theoretical distribution $P(G)$ (solid line) is obtained using the first two channels ($n = 2$) since the conductance values are not larger

than 4, indicating that no more than two different channels from each block Hamiltonian contribute to the conductance, while the ratio $s = L/l = 5.2$ is found to reproduce the numerical average conductance $\langle G \rangle = 1.2$. Fig. 2 (a) shows a good agreement between the theoretical (solid line) and numerical (blue histogram) distributions.

Let us now increase further the strength of disorder to $W = 600$ meV. In the presence of strong disorder, the main contribution to the conductance comes from a single transmission eigenvalue and therefore the multivariate distribution $P(\{\tau_i\})$ is simplified to the distribution of a single variable, $P(\tau)$. In this case, we can write an analytical expression for the probability density of the conductance $P(G)$ as:³⁷⁾

$$P(G) = C \frac{\text{acosh}^{1/2}(\sqrt{2/G})}{G^{3/2}(2-G)^{1/4}} \exp\left[(-l/L)\text{acosh}^2(\sqrt{2/G})\right], \quad (10)$$

where C is a normalization constant. As in the previous multichannel case, the ratio $s = L/l$ plays an important role since all the statistical properties of the conductance fluctuations are fixed by this ratio. For one channel, L/l can be extracted from the numerical simulations using $L/l = \langle -\ln(G/2) \rangle$. In Fig. 2(a), the conductance distribution (solid line) for $W = 600$ meV according to Eq. (10) is plotted. A good agreement between theory (solid line) and the numerical simulations (red histogram) is seen.

If we increase even further the strength of the disorder, the TIs reach the deeply insulating limit and the conductance distribution follows a log-normal distribution,^{35,36)} as shown for $W = 1000$ meV in Fig. 2 (b). The numerical distribution (histogram) for $\ln G$ is well described by $P(\ln G) = 1/\sqrt{2\pi\sigma^2} \exp[-(\ln G - \langle \ln G \rangle)^2/2\sigma^2]$ with $\sigma^2 = 2\langle -\ln G \rangle$. The value of $\langle \ln G \rangle$ has been obtained from the numerical calculations.

As we have pointed out, the BHZ Hamiltonian model belongs to the $\beta = 2$ symmetry class, however, for high energies ($E > 8$ meV) and disorder strength $W \sim 50$ meV, we notice in the phase diagram of Fig. 1 (c), δG approaches the value $\sqrt{8/15} \approx 0.73$ (yellow region), which corresponds to the UCF for the orthogonal symmetry ($\beta = 1$), i.e., the symmetry class for systems with TR symmetry and no spin orbit coupling (SOC). Furthermore, we have obtained the distribution of the conductance fluctuations at the point © in Fig. 1 (c) which, as shown in Fig. 2(c), follows a Gaussian distribution: the solid line corresponds to a Gaussian distribution with variance $8/15$, i.e., the variance value of the UCF for the orthogonal symmetry class. Additionally, to show the robustness of this result and contrast it with the conductance fluctuations for $\beta = 2$, in Fig. 3 we plot δG as a function of the disorder strength W at two different energies: $E = 6$ meV (blue squares) where the conductance standard deviation approaches the value 0.52, i.e., the $\beta = 2$ symmetry class and at $E = 20$ meV (red

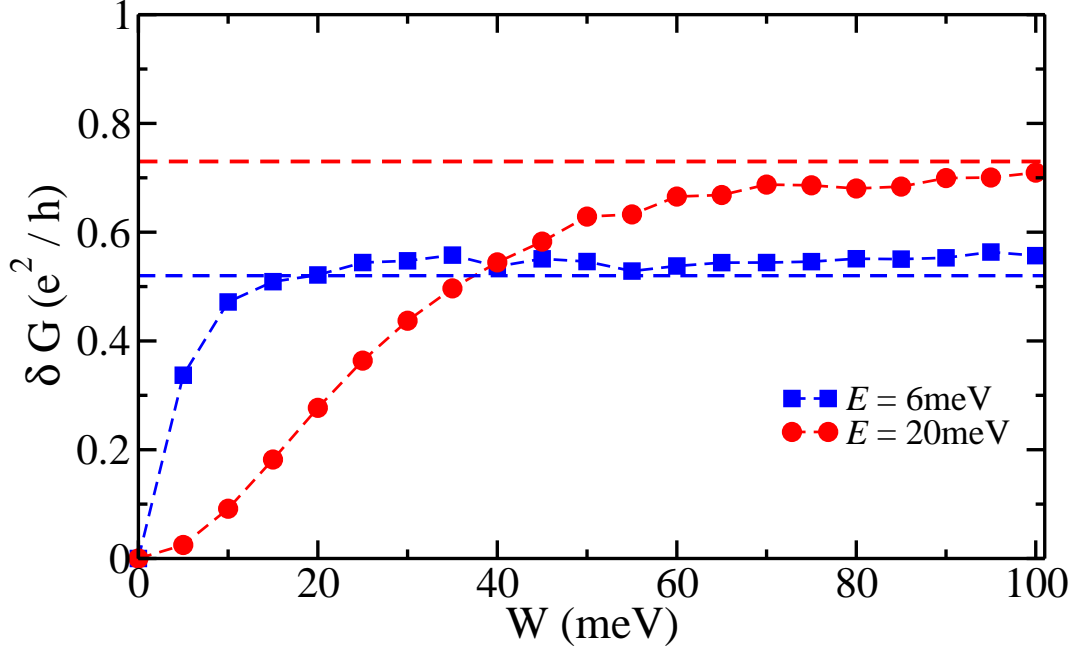


Fig. 3. (Color online) Standard deviation of the conductance δG as a function of the strength of the disorder W . At energy $E = 6\text{meV}$, δG is close to the UCF corresponding to the $\beta = 0.52$ symmetry class indicated with a blue dashed-line. However, at $E = 20\text{meV}$, δG approaches the value 0.73 (red dashed-line) that corresponds to the orthogonal case, symmetry class $\beta = 1$. Notice that we have chosen $E = 20\text{meV}$ which is not within the range of the phase diagram in Fig. 1, in order to clearly show a flat behavior of δG over a wide range of W .

dots), where δG is close to 0.73 that corresponds to the symmetry $\beta = 1$. This essentially reveals that effects of the SOC (off-diagonal terms in the Hamiltonian H_c) are negligible at high energies and strong disorder.^{38,39)}

3.3 Metal - Quantum Spin-Hall Crossover

In the M phase the conductance fluctuations follow a Gaussian distribution, as shown above. On the contrary, in the QSHI phase, there is no conductance fluctuations due to the robustness of the helical edge states against disorder. Thus, it is of interest to study the conductance fluctuations at the crossover between these two phases, when both edge and bulk states contribute to the conductance.

In our numerical simulations, we have chosen the point at the crossover: $W = 12, E = 4.55\text{ meV}$ (point \textcircled{D} in Fig. 1(b) and (c)). At this M-QSHI crossover point, we have analyzed the fluctuations of the first three largest different eigenvalues, represented by τ_1, τ_2 and τ_3 . We have verified numerically that these three channels give the main contribution to total conductance G i.e., the contribution of higher transmission channels is negligible. In the inset of Fig. 4(a) and 4(b), we show the distribution of each transmission eigenvalue for two different TI

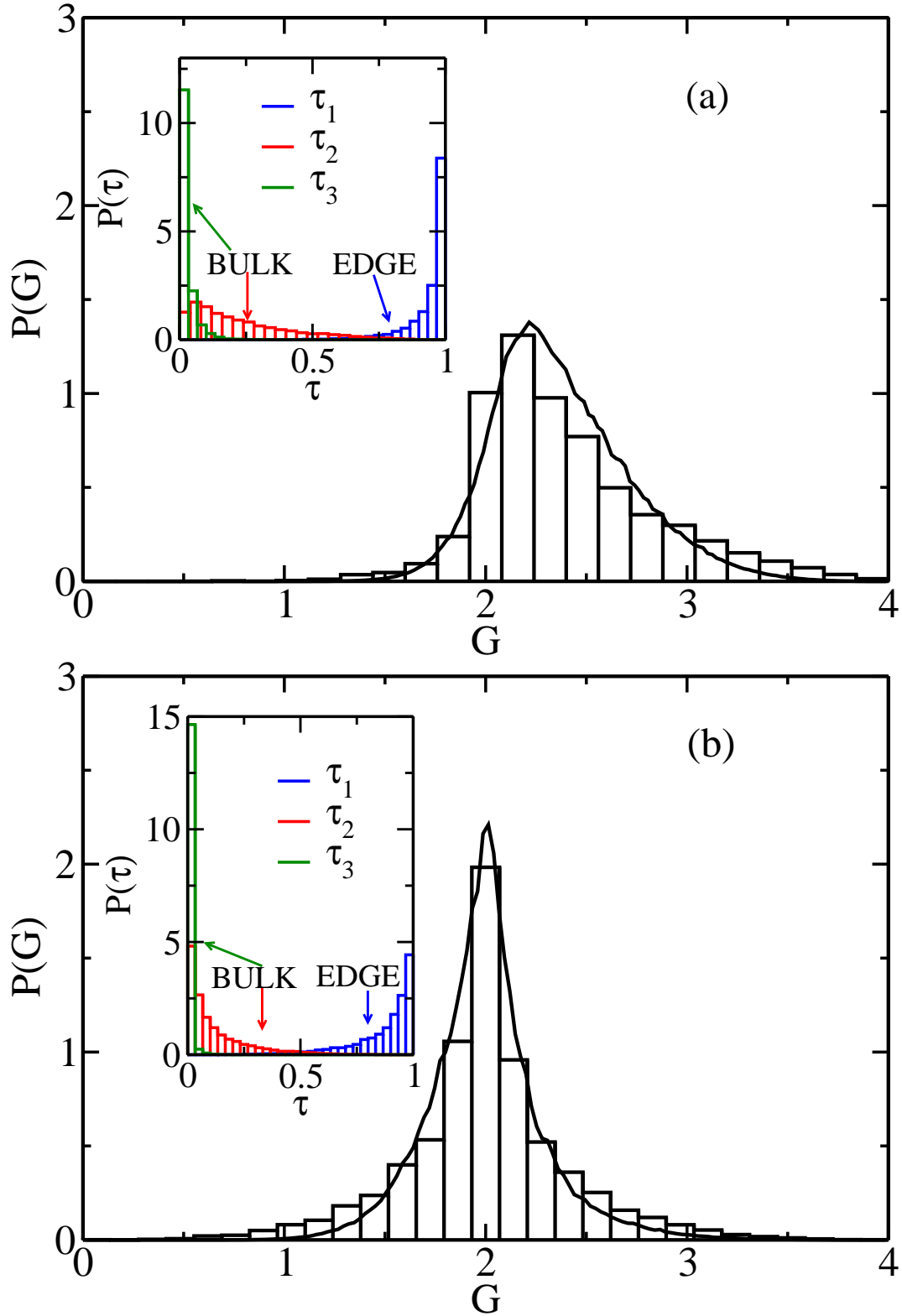


Fig. 4. (Color online) The conductance distribution with $\langle G \rangle = 2.39$ at the M-QSHI crossover at $E = 4.55$ meV and $W = 12$ meV for two different system lengths (a) $L=300$, corresponding to \textcircled{D} in the phase diagrams in Fig. 1 and (b) $L=600$. The solid line is the theoretical distribution. The probability distributions of the three largest transmission eigenvalues τ_1 , τ_2 , τ_3 are shown in the insets. For the distribution in (b), $\langle G \rangle = 1.99$ and $s_2 = 19s_1$, $s_3 = 44s_1$ with $s_1 = 0.34$.

wire lengths ($L = 300$ and 600 , respectively). We notice that the first transmission eigenvalue τ_1 , which is associated to the helical edge state, is highly transmitted, whereas the second and third transmission eigenvalues associated to the bulk states are poorly transmitted. Hence, the distribution of the first eigenvalue peaks at $\tau_1 = 1$, while the distribution of τ_2 and τ_3 , respectively, peaks at zero. This suggests that helical edge states are weakly localized, whereas bulk states are strongly localized. Therefore, in order to describe the conductance fluctuations within our theory, we need to introduce the information about the different strengths of localization of the edge and bulk states.

As we have pointed out above, the strength of the electron localization in our model is characterized by the parameter $s = L/l$ (see Eqs. (8) and (10)), which is determined by $\langle \ln G \rangle$ in the case of one transmission eigenvalue. Thus, in order to consider different localization strengths, we propose introducing a different s_i value for each transmission eigenvalue, which is extracted from the numerical calculations. For instance, for the distribution $P(G)$ shown in Fig. 4 (a), we found numerically that $\langle -\ln \tau_2 \rangle$ is 25 times larger than $\langle -\ln \tau_1 \rangle$, while $\langle -\ln \tau_3 \rangle$ is 60 times larger than $\langle -\ln \tau_1 \rangle$. Thus, we set $s_2 = 25s_1$ and $s_3 = 60s_1$ with $s_1 = 0.24$ fixed to reproduce the average conductance $\langle \ln G \rangle$, or equivalently $\langle G \rangle$. As an additional example, we show $P(G)$ for a longer TI wire ($L = 600$) in Fig. 4(b). Thus, the proposed method to calculate $P(G)$ needs a detailed analysis of the contribution of the different transmission eigenvalues, in contrast to the standard analysis where the knowledge of the conductance average, or the parameter s , is sufficient to obtain $P(G)$. Interestingly, distributions with similar landscapes at the M-QSHI crossover of a Z2 network model were reported in Ref. [23], where it was also found that the first largest transmission eigenvalues determine the conductance distributions. In Ref. [23], however, the network model belongs to the symplectic class ($\beta = 4$), whereas our case is for the unitary class $\beta = 2$. We thus conclude that the landscape of the conductance distribution is strongly determined by the different localization, and therefore different contribution to the conductance, of the transmission channels rather than the symmetry class.

3.4 Ordinary Insulator - Quantum Spin-Hall Crossover

As we have shown above, helical edge states are robust against disorder. However, at sufficiently strong disorder, edge states eventually become localized, leading the QSHI phase to an OI phase. At this crossover regime, but on the QSHI side, the conductance distribution has a large peak at $G = 2$, as shown in Figs. 5 (a) and 5 (b), because the edge states have not yet been fully localized. In contrast, on the OI side, the distribution shows a peak at $G = 0$ [see Figs. 5 (c) and 5 (d)], indicating that the edge states become localized.

To study the fluctuations on the QSHI side, we assume that the conductance fluctuations come from the edge states that start to penetrate into the 2D wire and whose conductance fluctuations can be described by Eq. (10), as in the OI phase. On the QSHI side, however, the maximum conductance of the edge states is 2; we thus only need to make the change of variable $G \rightarrow 2 - G$ in Eq. (10) to obtain the distribution of the conductance fluctuations:

$$P(G) = C \frac{\sqrt{\text{acosh} \sqrt{\frac{2}{2-G}}}}{(2-G)^{3/2} G^{1/4}} \exp \left[-s'^{-1} \text{acosh}^2 \sqrt{\frac{2}{2-G}} \right], \quad (11)$$

where C is a normalization constant and s' is determined by the average $s' = \langle \ln[(2-G)/2] \rangle$. Fig. 5 (a) and 5 (b) show $P(G)$ (solid line) given by Eq. (11) which agrees well with numerical simulations (histograms).

Regarding the OI to QSHI crossover, but on the OI side, the perfect conducting edge states become localized and the TI becomes an ordinary insulator. Thus, only a single transmission eigenvalue is relevant and the distribution of conductances is described by Eq. (10). Figs. 5 (c) and 5 (d) show both the numerical (histogram) and theoretical (solid line) distribution for $P(G)$.

4. Summary and Conclusions

Topological insulators are not free from impurities and/or lattice defects and therefore a full understanding of the effects of the disorder on the electronic transport is of interest from practical and fundamental points of view. We have studied the conductance fluctuations of disordered 2D TI wires modeled by the BHZ Hamiltonian with experimentally achievable parameters. We have been gone beyond the first moments of the conductance fluctuations and calculate analytically and numerically the complete distribution of the conductance.

The phase diagrams of the mean and the standard deviation of the conductance, which have been numerically obtained, show three different quantum phases or regimes: metal, quantum spin-Hall insulator, and ordinary insulator. We have obtained the conductance distribution in each regime as well as in their crossovers within a framework of random matrix theory. The conductance fluctuations follow the statistics of the unitary class $\beta = 2$ as a consequence of the block diagonal structure of the Hamiltonian, in which each block belongs to the unitary class $\beta = 2$. At strong disorder and high energies, we have found that the conductance fluctuations δG approach the value of the orthogonal universality class $\beta = 1$. We interpretate this result as a consequence of the fact that at high energies, the band structure of the TIs resembles that one of a normal metal and therefore the value of δG corresponds to case of

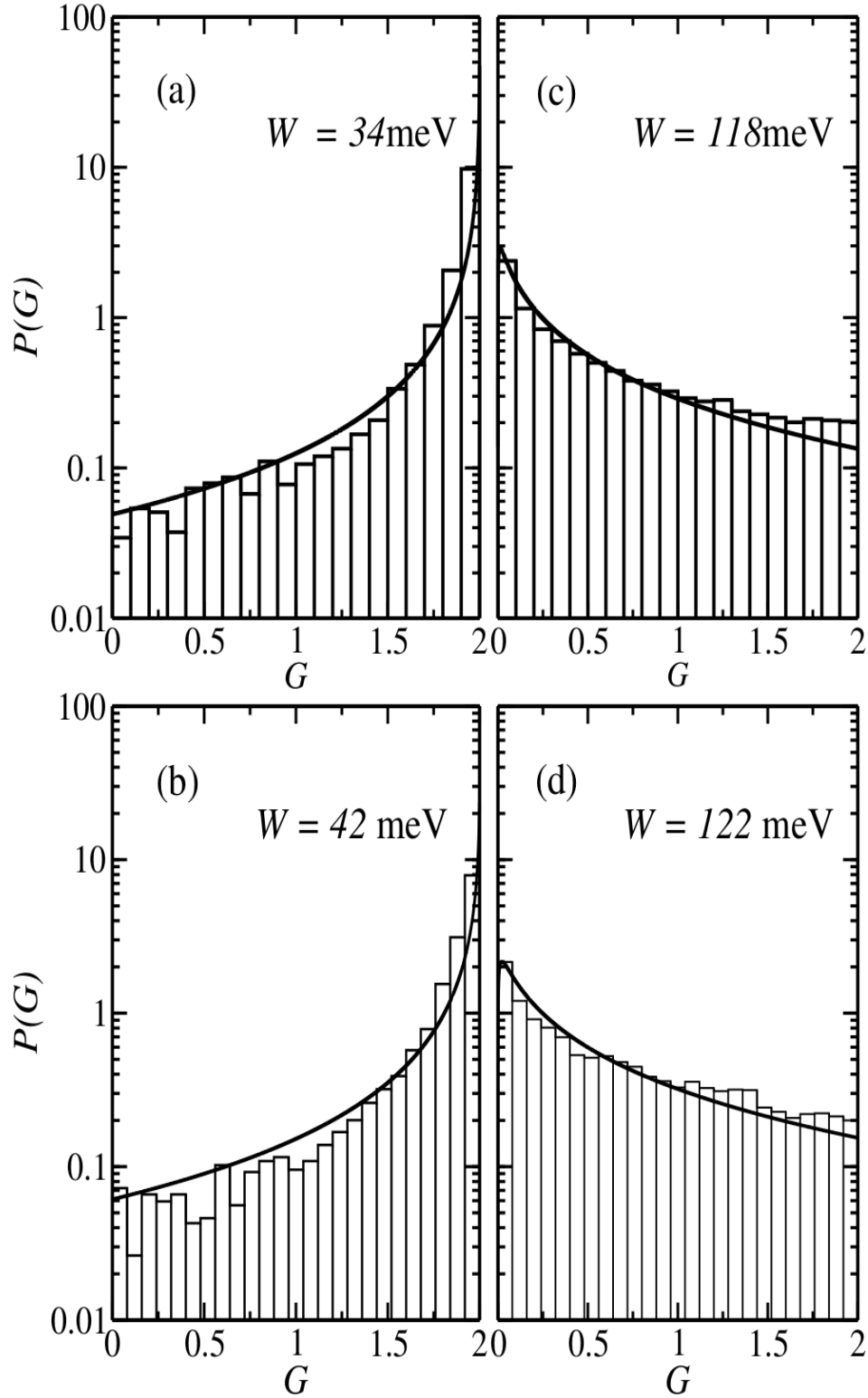


Fig. 5. Conductance distributions at the QSHI-OI crossover on the QSHI side [panels (a) and (b)] and on the OI side [panels (c) and (d)]. The distributions in panels (a) and (c) correspond to the points \textcircled{E} and \textcircled{F} in the phase diagram in Fig. 1, at $E = 4$ meV. For the panels (b) and (d) $E = 3.8$ meV. Histograms and solid lines curves correspond to the numerical and theoretical distributions: Eq. (10) with $s = 2.03$ (a), $s = 1.86$ (b) and Eq. (11) with $s' = 3.6$ (c), $s' = 3.22$ (d).

the orthogonal universality class, as long as the disorder is sufficiently strong to wash out the SOC effects. We have actually numerically verified that the value of conductance fluctuations ($\beta = 1$) is not affected by the strength of the SOC.

Furthermore, our results reveal that at M-QSHI and OI-QSHI crossover regimes, the presence of the helical edge states play a crucial role in the conductance statistics. At those crossover regimes, both bulk and helical edge states contribute to the conductance, albeit with different extent of localization. Consequently, the conductance distributions change drastically from one quantum phase to another one due to the different degree of localization of the helical edge and bulk states, as well as the number of relevant transmission channels.

We believe that the extensive analysis of the conductance fluctuations presented here gives a complete picture of the statistics of the conductance fluctuations and offers deeper insights into the quantum transport in disordered TIs.

Acknowledgment

H.-C. H. would like to thank Dong-Hui Xu for helpful discussions. V. A. G thanks R. A. Molina for helpful suggestions and discussions. V. A. G acknowledges support from MINECO (Spain) under the Project number FIS2015-65078-C2-2-P and Subprograma Estatal de Movilidad 2013-2016 under the Project number PRX16/00166. He also thanks The Physics Department and the Center for Theoretical Sciences of the National Taiwan University, as well as the Physics Department of Queens College, The City University of New York for the hospitality. H.-C. H., I. K. and G.-Y. G. acknowledge support from Academia Sinica, National Center for Theoretical Sciences and the Ministry of Science and Technology of The R.O.C. The authors gratefully acknowledge the resources from the supercomputer “Terminus”, technical expertise and assistance provided by the Institute for Biocomputation and Physics of Complex Systems (BIFI) - Universidad de Zaragoza as well as from the National Center of High-performance Computing of Taiwan.

References

References

- 1) X.-L. Qi and S.-C. Zhang, *Rev. Mod. Phys.* **83**, 1057 (2011).
- 2) C. L. Kane and E. J. Mele, *Phys. Rev. Lett.* **95**, 226801 (2005).
- 3) M. Z. Hasan and C. L. Kane, *Rev. Mod. Phys.* **82**, 3045 (2010).
- 4) T.-W. Chen, Z.-R. Xiao, D.-W. Chiou, and G.-Y. Guo, *Phys. Rev. B* **84**, 165453 (2011).
- 5) B. A. Bernevig, T. L. Hughes, and S. C. Zhang, *Science*, **314**, 1757 (2006).
- 6) H. Jiang, L. Wang, Q.-f. Sun, and X. C. Xie, *Phys. Rev. B* **80**, 165316 (2009).
- 7) J. Li, R.-L. Chu, J.K. Jain and S.-Q. Shen, *Phys. Rev. Lett.* **102**, 136806 (2009).
- 8) K.-I. Imura, Y. Kuramoto, and K. Nomura, *Phys. Rev. B* **80**, 085119 (2009).
- 9) C.-Z. Chen, H. Liu, H. Jiang, Q.-F. Sun, Z. Wang, and X. C. Xie, *Phys. Rev. B* **91**, 214202 (2015).
- 10) Y. Zhang and A. Vishwanath 2010 *Phys. Rev. Lett.* **105**, 206601 (2010).
- 11) J. H. Bardarson, P. W. Brouwer, and J. E. Moore, *Phys. Rev. Lett.* **105**, 156803 (2010).
- 12) S. Cho, B. Dellabetta, R. Zhong, J. Schneeloch, T. Liu, G. Gu, M. J. Gilbert, and N. Mason 2015 *Nat. Commun.* **6**, 8634 (2015).
- 13) R. Du, H.-C. Hsu, A. C. Balram, Y. Yin, S. Dong, W. Dai, W. Zhao, D. S. Kim, S.-Y. Yu, J. Wang, X. Li, S. E. Mohny, S. Tadigadapa, N. Samarth, M. H. W. Chan, J. K. Jain, C.-X. Liu, and Q. Li, *Phys. Rev. B* **93**, 195402 (2016).
- 14) Y. Imry, *Introduction to Mesoscopic Physics* (Oxford University Press, Oxford, 1997).
- 15) C. Beenakker, *Rev. Mod. Phys.* **69**, 731 (1997).
- 16) P. A. Lee and A. D. Stone, *Phys. Rev. Lett.* **55**, 1622 (1985).
- 17) S. Matsuo, K. Chida, D. Chiba, T. Ono, K. Slevin, K. Kobayashi, T. Ohtsuki, C.-Z. Chang, K. He, X.-C. Ma and Q.-K. Xue, *Phys. Rev. B* **88**, 155438 (2013).
- 18) A. Kandala, A. Richardella, D. Zhang, T. C. Flanagan, and N. Samarth, *Nano Lett.* **13(6)**, 2471 (2013).
- 19) Z. Li, Y. Meng, J. Pan, T. Chen, X. Hong, S. Li, X. Wang, F. Song and B. Wang, *Appl. Phys. Express*, **7**, 065202 (2014).
- 20) Z. Li, T. Chen, H. Pan, F. Song, B. Wang, J. Han, Y. Qin, X. Wang, R. Zhang, J. Wan, D. Xing and G. Wang, *Sci. Rep.* **2**, 00595 (2012).
- 21) Y. Takagaki, *Phys. Rev. B* **85**, 155308 (2012).

- 22) D.-H. Choe, and K. J. Chang, *Sci. Rep.* **5**, 10997 (2015).
- 23) K. Kobayashi, T. Ohtsuki, H. Obuse, and K. Slevin, *Phys. Rev. B* **82**, 165301 (2010).
- 24) D. Xu, J. Qi, J. Liu, V. Sacksteder, X. C. Xie, and H. Jiang, *Phys. Rev. B* **85**, 195140 (2012).
- 25) I. Knez, and R. Du, *Front. Phys.* **7**, 200 (2012).
- 26) C. X. Liu, T. L. Hughes, X.-L. Qi, K. Wang, and S. C. Zhang, *Phys. Rev. Lett.* **100**, 236601 (2008).
- 27) P. A. Mello and N. Kumar, *Quantum Transport in Mesoscopic Systems: Complexity and Statistical Fluctuations* (Oxford University Press, Oxford, 2004).
- 28) In the ballistic regime, RMT has been also successfully applied to investigated the conductance fluctuations in chaotic quantum dots based on graphene or TIs materials: T. C. Vasconcelos, J. G. G. S. Ramos, and A. L. R. Barbosa, *Phys. Rev. B* **93**, 115120 (2016).
- 29) D.-H. Xu, J.-H. Gao, C.-X. Liu, J.-H. Sun, F.-C. Zhang, and Y. Zhou, *Phys. Rev. B* **89**, 195104 (2014).
- 30) We point out that, contrary to the model studied here, in the so-called topological Anderson insulator introduced in 7, there is no inversion of the bands (the mass term was fixed to a positive value), i.e., edge states are absent, in the clean limit. The existence of edge states was shown at intermediate values of the disorder strength.
- 31) J. R. Bindel, M. Pezzotta, J. Ulrich, M. Liebmann, E. Ya. Sherman, and M. Morgenstern, *Nature Physics* **12**, 920 (2016).
- 32) S. Datta, *Electronic transport in mesoscopic systems* (Cambridge University Press, Cambridge, England, 1995).
- 33) C. H. Lewenkopf and E. R. Mucciolo, *J. Comput. Electron.* **12**, 203 (2013).
- 34) F. Haake, *Quantum Signatures of Chaos* (Springer Heidelberg Dordrecht London New York, 2010)
- 35) C. W. J. Beenakker, and B. Rejaei, *Phys. Rev. Lett.* **71**, 3689 (1993).
- 36) K. A. Muttalib, P. Wölfle, V. A. Gopar, *Annals of Physics* **308**, 156 (2003).
- 37) V. A. Gopar and R. A. Molina, *Phys. Rev. B* **81**, 195415 (2010).
- 38) We have verified numerically that statement: At $E = 20\text{meV}$ we have calculated the standard deviation δG at different values of the SOC ($A = 18.5, 12, \text{ and } 6 \text{ meV}$) and noticed that δG is not affected, i.e., $\delta G \sim 0.73$ in all cases. In contrast, at low energies,

for instance at $E = 6\text{meV}$ the fluctuations of the conductance depend on the value of the SOC.

- 39) A change in the size of the conductance fluctuations from $\beta = 4$ to $\beta = 1$ symmetry classes due to the presence of disorder has been reported in quantum wires with strong spin-orbit interaction: T. Kaneko, M. Koshino and T. Ando, Phys. Rev. B **81**, 155310 (2010).